Heliyon 9 (2023) e20748

Contents lists available at ScienceDirect

Heliyon

journal homepage: www.cell.com/heliyon

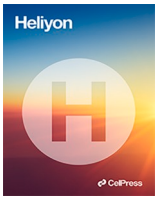

Influence of boron doping level and calcination temperature on hydrogen evolution reaction in acid medium of metal-free graphene aerogels

J. Cencerrero [a], P. Sánchez [a], A. de Lucas-Consuegra [a], A.R. de la Osa [a], A. Romero [b,*]

[a] *Department of Chemical Engineering, Technical School of Agronomic Engineers. University of Castilla-La Mancha, Avda. Camilo José Cela 12, 13071, Ciudad Real, Spain*

[b] *Faculty of Chemical Sciences and Technologies, Technical School of Agronomic Engineers. University of Castilla-La Mancha, Avda. Camilo José Cela 12, 13071, Ciudad Real, Spain*

A R T I C L E I N F O

Keywords:
Hydrogen evolution reaction
Heteroatom doped graphene
3D graphene aerogels
Metal free electrocatalysts
Boron-doping

A B S T R A C T

In this work, metal-free boron-doped graphene-based aerogels were successfully synthesized *via* a one-step autoclave assembly followed by freeze-drying and used as electrocatalysts for the hydrogen evolution reaction (HER) in acidic media. The synthesized reduced graphene oxide aerogels (rGOA) showed improved electrocatalytic activity by introducing boron and structural defects. The amount of boric acid used both as a dopant and reducing agent in the synthesis was optimized (boric acid/GO mass ratio = 17.5) to practically reach the crystallization limit of boric acid (boric acid/GO mass ratio = 20). It was observed that the higher the amount of boric acid added, the more boron was incorporated into the carbonaceous structure, improving the electrocatalytic activity of the final aerogel. Furthermore, calcination of the boron-doped electrocatalyst at 600 °C resulted in final aerogels with low oxygen content, moderate surface area, bimodal pore size distribution, and a high electrochemical active surface area. The final 3D graphene aerogel developed in this work, showed such outstanding electrocatalytic activity in HER as to replace noble metal-based electrocatalysts in the future.

1. Introduction

Due to decreasing fossil energy reserves and their high greenhouse gas production, the use of green hydrogen as alternative energy is getting significant attention [1,2], because of green hydrogen is an energy vector with high energy density and pollution-free production [3]. Currently, a clean and reliable way to obtain pure hydrogen is the electrocatalytic water splitting that combine the Hydrogen Evolution Reaction (HER), where the H_2 is produced, and the oxygen evolution reaction (OER), where it is obtained the electrons. Traditionally the water splitting reaction has been carried out by means of the use of Pt-based electrocatalyst due to the large overpotential and sluggish kinetics of OER and HER process [4]. However, research is currently underway to develop different critical aspects of the process, such as the use of metal-free electrocatalysts and the oxidation of alcohols (such as the Ethanol Oxidation Reaction, EOR [5]) as an alternative to reduce the overpotential of the OER. Focusing on the HER, the mechanism of this reaction depends on the pH of the media when the reaction is being carried out. When the media is acid, the HER mechanism is based on three

* Corresponding author.
E-mail address: amaya.romero@uclm.es (A. Romero).

https://doi.org/10.1016/j.heliyon.2023.e20748
Received 5 July 2023; Received in revised form 29 September 2023; Accepted 5 October 2023
Available online 12 October 2023

mechanism reaction that depend on the potential applied in the surface of the catalyst. The first reaction taking the potential into account is the Volmer's reaction, which consider the adsorption of the proton $H_3O^+ + e^- \rightarrow H_{ads} + H_2O$ (theoretical Tafel slope ≈ 120 mV/dec). The second reaction is the Tafel reaction $H_{ads} + H_{ads} \rightarrow H_2 \uparrow$ (theoretical Tafel slope ≈ 40 mV/dec), and finally the Heyrovsky reaction $H_3O^+ + e^- + H_{ads} \rightarrow H_2 \uparrow + H_2O$ (theoretical Tafel slope ≈ 30 mV/dec) [6]. However, the industrial application of the overall process of water splitting is limited due to the high price and low availability of the noble metals used in the electrocatalyst of this reaction, as well as its poor stability in neutral, alkaline, and acidic electrolytes [7–12]. Thus, a high-efficiency, low-cost and stable metal-free HER electrocatalysts are urgently necessary to replace the traditional Pt-based ones.

Recent studies suggest that metal-free electrocatalyst based on graphene derivatives might be an efficient option to replace Pt-based electrocatalysts in HER [13,14]. Graphene is a 2D material composed of a sequence of carbon atoms connected by covalent bonds with sp^2 hybridized carbons. This fact, generate a stable and regular hexagonal patter that has low Joule effect and high electrical conductivity [14]. The problem of graphene-derivatives is that the graphene layers could stack up generating mass transfer problems and a decrease of the electrochemical activity. To solve this, graphene aerogels materials are being developed, which are similar to reduced graphene oxide but with a 3D low density structure, with exceptional textural, electrical and thermal properties because of their graphene building blocks [14,15]. Graphene-based aerogels can be developed by hydrothermal processes in which the high pressure and temperature used, allow the graphene sheets to assemble into stable porous structures [16]. After the 3D structure has been built, a drying method is needed to prevent the structure from collapsing (supercritical drying [17] or freeze-drying [18,19]).

On the other hand, in order to obtain higher cathodic currents in HER, the carbon matrix of graphene-based aerogels can be modified by introducing certain heteroatoms that enhance the electrocatalytic activity [20]. Several heteroatoms have been used in bibliography as dopants such as N, B, S, P, etc., to improve the activity of graphene-based electrocatalyst [21–25]. Among them, boron is the less used so far and therefore more novel. It has an equivalent size and bond length compared to C–C, so it does not cause much distortion in the planar structure of graphene, unlike other heteroatoms such as nitrogen [26]. The distortion of carbon lattice symmetry opens the catalyst band gap, generating semiconducting properties. In particular, boron doping generates p-type semiconductors [27]. B doping generate charging-induced asymmetric spin distributions in the p-system of graphene and, this fact, enhances electrocatalytic activity [28], as observed by Yang et al. [29], who generated a boron-doped graphene using a hydrothermal process achieving a overpotential (mV) at 10 mA cm^{-2} (η_{10}) of 260 mV.

The calcination temperature is an important parameter in doped graphene electrocatalysts. Recently, Jung et al. [30] demonstrated how a final calcination step generated changes in the specific surface area, bonding configuration, conductivity and boron and oxygen contents of the electrocatalyst, showing better electrochemical results.

It follows from the above that a scalable method is required to produce new metal-free electrocatalysts that avoid the use of metal in the production of green hydrogen. Thus, in this work, a systematic and in-depth study was carried out to investigate the influence of the dopant (B) content and the calcination temperature on the electrocatalytic activity for HER in acidic media of the synthesized graphene-based aerogels. The final 3D graphene aerogel developed in this work, which has a large surface area and low density, showed such outstanding electrocatalytic activity in HER as to replace noble metal-based electrocatalysts in the future.

2. Experimental

2.1. Materials

Graphite powder 99% purity (Ø<20 μm), sulfuric acid 96–98% (H_2SO_4), potassium permanganate ($KMnO_4$), hydrochloric acid ≥37% (HCl) and boric acid (H_3BO_3), were supplied by Aldrich. Ethanol 99.5% (CH_3–CH_2OH) and hydrogen peroxide 33% (H_2O_2) were supplied by Panreac.

2.2. Synthesis of the graphene-based aerogels

2.2.1. Graphite oxidation

Graphite oxide (GO) was synthesized using the Improved Hummer's Method optimized by Lavin-Lopez et al. [31]. A mixture of 45 g of $KMnO_4$ and 15 g of graphite was added to 400 mL of H_2SO_4 under continuous agitation for 3 h and 50 °C. To stop the reaction, 3 mL of H_2O_2 and 400 g of flake ice the mixture was added to the mixture. Then, the mixture was filtered under vacuum and washed with 200 mL of deionized water, ethanol and HCl. Finally, the cake was dried for 3 h under 60 °C.

2.2.2. Synthesis of boron graphene-based aerogels

First, a mixture of 0.8 g of GO mixed with 400 mL of deionized water was sonicated and then, it was added the appropriate amount of reducing agent (boric acid [32]) and stirred for 15 min at 900 rpm. Then, the mixture was poured into an autoclave to carry out the hydrothermal process. The autoclave was heated for 12 h at 180 °C (10 °C/min). The obtained graphene hydrogels were freeze-dried for 15 h at −70 °C and at 0.08 mbar to obtain the final aerogels. Finally, the aerogels were calcined at different temperatures.

To optimize the required amount of reducing agent, different syntheses were carried out by varying the boric acid/GO mass ratio (12.5–20). The resulting samples were named as x-BrGOA where x is the boric acid/GO mass ratio. Thus, it was used 10 g, 12 g, 14 g and 16 g of boric acid, generating the aerogels 12.5-BrGOA, 15-BrGOA, 17.5-BrGOA and 20-BrGOA, respectively. Finally, the influence of the calcination temperature was studied on the selected optimal electrocatalyst by varying the calcination temperature between 400 and 800 °C. Resulting samples were named as 400B, 600B and 800B.

2.3. Physicochemical characterization techniques

HRSEM imaging was performed with a PIN-diode BSE detector by ZEISS GeminiSEM 500 FE-SEM. Elemental analyses were performed by a LECO CHNS-932 equipment. The amount of C, H and N was measured after being full oxidized followed by total and instantaneous combustion. The oxygen content was then determined by the difference. Boron content incorporated to the aerogels was analysed by Inductively Coupled Plasma (ICP). Fourier transform infrared (FTIR) analysis were carried out on a SPECTRUM TWO spectrometer (PerkinElmer, Inc). Furthermore, this was performed in transmission mode using ZnSe (550-6000 cm^{-1}) and KBr (350-8300 cm^{-1}) pellets. Density of the samples were measured using a nitrogen picnometry in standard conditions on an Ultrapyc 1200 pycnometer (Quantachrome Instruments). In this analysis, the changes in pressure between the samples without and with nitrogen was quantified and, assuming that nitrogen atoms can penetrate all the open pores in the material, the skeletal volume was measured. Textural properties were measured using nitrogen as the sorbate gas in a Quantachrome Quadrasorb SI system at 77 K. Pore size distributions, obtained with the BJH method, and total surface areas, obtained by the multipoint BET method, were firstly obtained from the N_2 adsorption/desorption measurements. The XRD analysis were obtained with a diffractometer (PHILIPS, PW-1711) with CuK_a radiation (l = 0.15404 nm). The in-plane crystallite size (L_A) and the crystal stack height (L_c) were the crystallographic parameters that were evaluated as presented in the supporting information. The XPS analysis were carried out in a Thermo Scientific Multilab 2000 spectrometer fitted with a 110 mm hemispherical sector analyzer and a dual-anode X-Ray source (Al Kalpha and Mg K alpha with photon energies 1486.7 and 1253.6 eV, respectively). Each sample was supported on a sample stub using a copper double adhesive tape before entering to FEAL chamber to degass for 1 day. Survey spectra and high-resolution core level spectra were measured using the Mg kalpha X-ray source at 400 W and 15 eV pass energy. The core level spectra were fitted and deconvolute using the CASAXPS software package. No surface sputtering with Ar ions was done and all the measurements were made on as-received samples.

2.4. Electrochemical measurements

The electrochemical analyses were conducted in a three-electrode half-cell system, with a glassy carbon rotating disk electrode (Metrohm Hispania, 5 mm internal diameter) as the working electrode, a carbon rod as the counter electrode, and a saturated Ag/AgCl (3 M KCl) as the reference electrode. Catalyst inks were prepared by mixing 2 mg of catalyst, 250 μL of water, 750 μL of isopropanol, and 8 μL of Nafion 5 wt%. Then, 19 μL of the ink was deposited onto the working electrode to generate a catalytic loading of 0.2 mg cm^{-2}.

For HER behaviour, Linear Sweep Voltammetries (LSV) analysis were obtained in a rotation of 1900 rpm at a 5 mV s^{-1} scan rate, and the Tafel plots were obtained from these LSVs. To maintain the solution inert, it was deaerated for 15 min by N_2 bubbling and it was maintained over the solution during all tests.

Double-layer capacitance (C_{dl}) was determined by using cyclic voltammetries (CV), which were carried out in a potential range where there are not faradaic processes (0.1–0.3 V for HER). C_{dl} were obtained from the relation of capacitive currents ($\Delta J = J_{Anodic} - J_{Catodic}$) at 0.15 V vs RHE at different scan rates (10, 20, 30, 40 and 50 mV s^{-1}) of the previous CVs essays [33,34].

3. Results and discussion

3.1. Influence of the amount of B-heteroatom doping

The synthesis of B-doped graphene aerogels electrocatalysts (B-rGOA) using different amounts of boric acid (reducing agent) allows to incorporate different amounts of B into the final aerogel and thus, to analyse its influence on the electrochemical activity and physicochemical properties. To this end, the reductant (g)/GO(g) ratio was varied between 12.5 and 20.

Table 1 shows the elemental composition of the different aerogels synthesized. As expected, as the higher amount of reducing agent, the greater elimination of oxygenated functional groups (reduction degree) was achieved. Likewise, an addition of higher amount of reducing agent resulted in higher boron doping. Note that for sample 20-BrGOA, the elemental composition could not be determined because the high amount of reducing agent used caused the boron to crystallise outside the material, as will be confirmed later by SEM images. Because of the presence of boron crystals and the incorrect GO reduction during the synthesis, sample 20-BrGOA was not considered in the study.

Fig. 1 shows the FITR analysis of the aerogels synthesized using different amounts of boric acid. Characteristic bands associated to the different oxygen groups appear in the spectra, such as C–O (1050-1100 cm^{-1}), C═O groups (around 1700 cm^{-1}) [35], C–OH

Table 1
Elemental composition (wt.%) of boron-doped graphene aerogels (GrO is showed with comparative purposes).

Samples	C	H	O	B
GrO	43	3	50	–
12.5-BrGOA	55	2	42	1
15-BrGOA	64	1	31	4
17.5-BrGOA	64	2	27	7
20-BrGOA	–	–	–	–

groups (around 1400 cm^{-1}) [20] and the bond of the functional group C–O–C (around 1200 cm^{-1}) [35]. The peak associated with the C═C group (1600-1630 cm^{-1}) [36] was clearly observed due to the materials maintain the sp^2 hybridization of the carbonaceous matrix. Also, several peaks were observed in the 2050-2400 cm^{-1} region attributed to the –C≡C- and the 2700-2900 cm^{-1} signal related to the C–H groups [37]. The peak located at 3220 cm^{-1}, which corresponds to the vibration of the B–O bond, confirms the boron-doping and corroborates the information given by the elemental analysis [38]. As observed, in relation to the characteristic peaks of each of the oxygen functional groups, no significant differences were observed between the samples.

Fig. S1 shows the XRD analysis corresponding to the different synthesized aerogels. The three samples show an intense characteristic peak at $2\theta = 25°$, which corresponds to the (0 0 2) plane, that indicates the presence of π-π stacking interaction between the graphene sheets, because of the partial restoration of the sp^2 graphitic network originated by the GO reduction [39], which could be corroborated by the presence of the intense C═C signal in the FTIR. A weaker peak appears at $2\theta = 43°$ in all three samples, which corresponds to the crystallographic plane (1 0 0), indicating disordered stacking of graphene sheets [40].

Table 2 shows the textural properties and crystalline parameters of the different aerogels prepared in this study. It can be observed that no remarkable changes in pore volume size and surface area were observed until a high amount of boric acid was added in the synthesis (17.5-BrGOA), which is expected to improve its electrocatalytic activity for the HER reaction [41]. Furthermore, no significant changes were observed either in the crystallinity parameters or in the density values of the studied samples.

Fig. 2 (a – c) and Fig. S2 show the pore size distribution and the N_2 adsorption-desorption isotherms of the synthesized aerogels, respectively. As for the adsorption/desorption isotherm, in general they can be classified as group IV isotherms, which present a hysteresis loop of type H3 (associated with capillary condensation of the pore [20]) appearing at a relative pressure (P/P_0) close to 0.5 which demonstrates the existence of mesopores [42]. It can be seen in the pore size distribution that, a bimodal distribution of porous is presented in the three aerogels with a high presence of mesopores, which can improve the mass transfer processes [20]. Furthermore, the higher amount of reductant (boric acid) added to the synthesis, the more amount of mesoporous in the aerogel (17.5-BrGOA), which explain the higher surface area and pore volume values commented before.

An in-depth analysis of the graphene-based morphology is shown in Fig. 3 (a-d) using the SEM pictures. It can be seen how in the 20-BrGOA sample, boron crystals were generated, which remained anchored in the structure without reducing it. In the other samples, a porous structure made up of both mesopores and micropores generated by the randomly assembly of the 2D graphene layers, can be observed. Moreover, as previously mentioned, the 17.5-BrGOA sample showed a more developed porous structure.

Heteroatom-doping in the carbon matrix is well-known for generate electrochemical enhancements [43], but the different bonds generated between the carbon of the graphene and the heteroatom is crucial. The XPS spectra of the boron-doped graphene aerogels are shown in Fig. 4 (a – c) and Table 3. Peaks at 193.5 and 192.75 eV confirm the presence of B in the sample, being the first peak related to the connection of the B to an atom of O (B–O) and the other one related to the substitution of a carbon atom for one of B in the graphene layer (BC_2O) [32]. In addition, the substitution of the C atom by the B atom, generating the BC_2O bond, is related to the generation of structural defects in the carbonaceous matrix [44], and this is associated with improvements of the electrochemical activity of the final aerogel [45]. In this sense, the enhancement in the oxygen functional groups reduction, previously seen by elemental analysis, was also confirmed by XPS. The high intensity of the B1 (B–O bond) in sample 12.5-BrGOA confirms that the lower amount of reductant used in the synthesis results in a higher presence of oxygen functional groups in the final aerogels. Furthermore, both B1 and B2 bonds in 17.5-BrGOA sample appeared at lightly higher binding energy, which indicates that these bonds are more stable in this sample [46].

To determine the electrocatalytic activity of the synthesized electrocatalysts, Fig. 5a shows the respective LSVs. Compared to

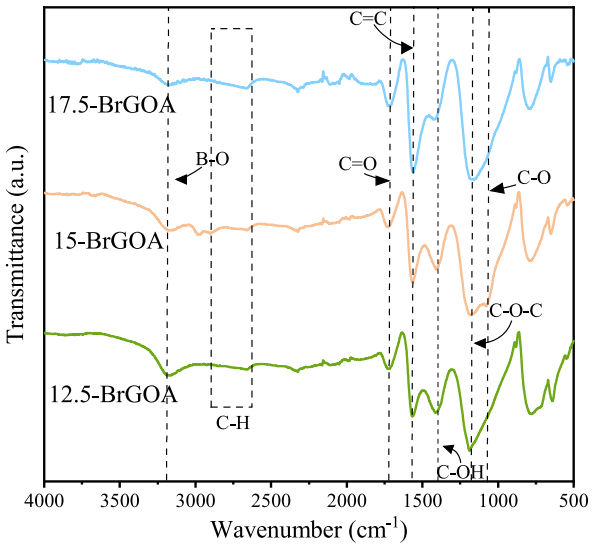

Fig. 1. FTIR analysis of boron-doped graphene aerogels.

Table 2
Crystallographic parameters, textural properties and density of boron-doped graphene aerogels.

Samples	L_C (nm)	L_A (nm)	Total pore volume (cm^3/g)	Surface area (m^2/g)	Density (mg/cm^3)
12.5-BrGOA	1.3	3.5	0.9	110	1.2
15-BrGOA	1.4	3.8	0.9	105	1.2
17.5-BrGOA	1.4	3.8	1.1	163	1.1

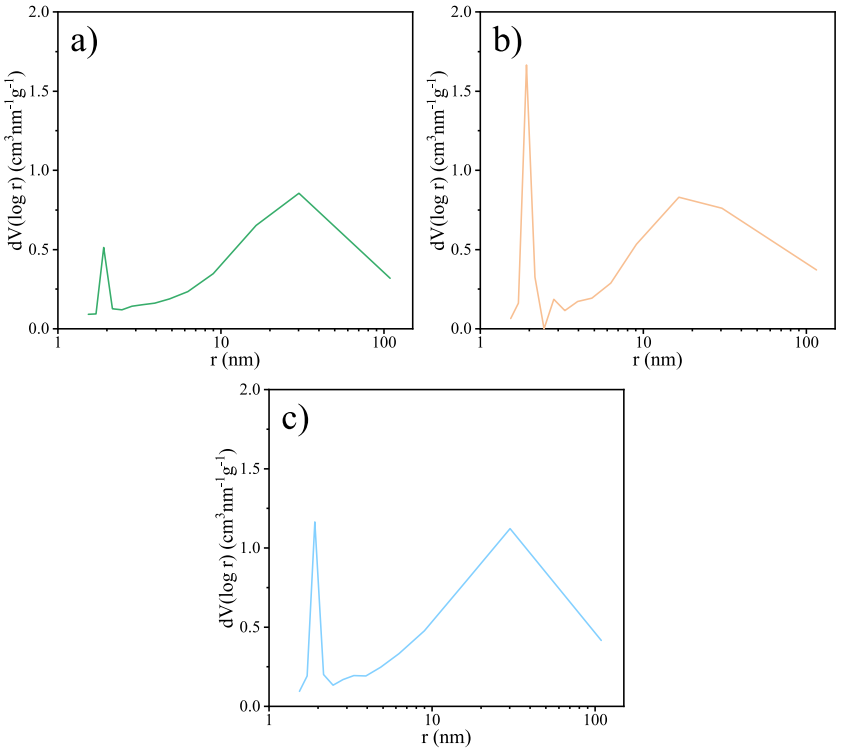

Fig. 2. Pore size distribution of a) 12.5-BrGOA, b) 15-BrGOA and c) 17.5-BrGOA.

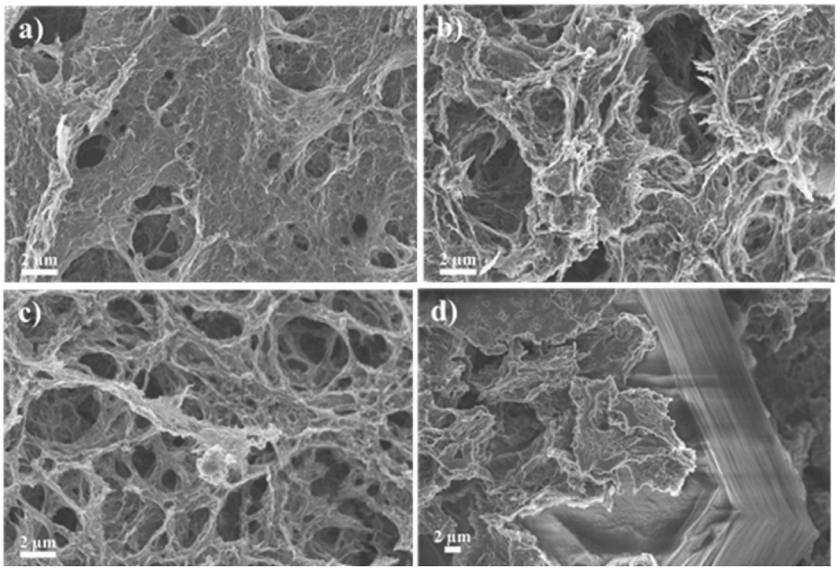

Fig. 3. SEM pictures of a) 12.5-BrGOA, b) 15-BrGOA, c) 17.5-BrGOA and d) 20-BrGOA.

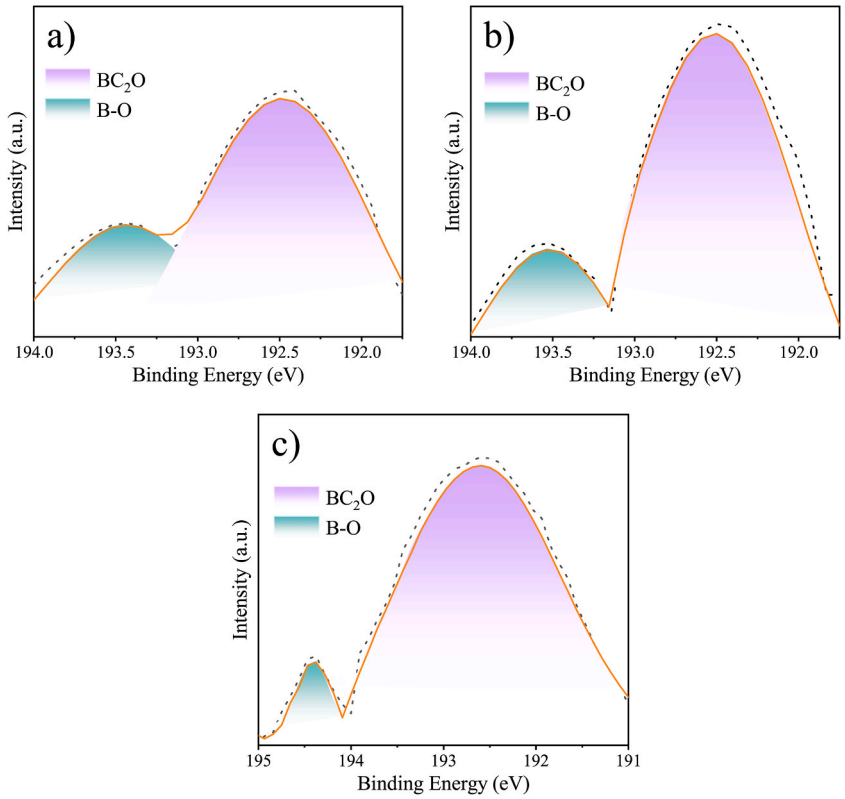

Fig. 4. Core level high-resolution B1s XPS spectra of a) 12.5-BrGOA, b) 15-BrGOA and c) 17.5-BrGOA.

Table 3
Element content (%) and fitted results of B1s core level XPS spectra of X-BrGOA graphene aerogels.

	Element content (%)			% Boron functional groups (BE, eV)[a]	
Samples	C	O	B	B1 (193.7)	B2 (192.6)
12.5-BrGOA	73	26	1	40	60
15-BrGOA	74	22	4	35	65
17.5-BrGOA	74	21	5	10	90

[a] Notes. B1: B–O, B2: BC_2O.

commercial 20%Pt/C, the aerogel that showed the best electrocatalytic activity was 17.5-BrGOA (η_{10} = 105 mV), which has been attributed to the presence of a higher proportion of boron in the structure of the carbonaceous material that allows to improve the p-type conductive behaviour. Also, 17.5-BrGOA was the one that showed a larger pore volume and a larger surface area compared to the other samples, allowing it to provide many active sites for the HER reaction to take place [47]. Fig. 5b shows the corresponding Tafel slopes. As expected, the electrocatalyst that obtained the lowest slope (64 mV dec^{-1}) was 17.5-BrGOA, considering 20%Pt/C with a value of 30 mV dec^{-1} as reference. A smaller Tafel slope means a faster kinetic process, indicating that the catalyst can achieve the desired current at a lower overpotential. The C_{dl} measurements (obtained of the CVs essays, Fig. S3), showed in Fig. 5c, were in line with the LSV results, obtaining the sample 17.5-BrGOA the greatest C_{dl} value (9.5 mF cm^{-2}). This fact indicates that this electrocatalyst has a larger number of active centres and thus, better electrochemical performance [48].

Considering the obtained results, the graphene-based aerogel 17.5-BrGOA was selected as the optimum for subsequent optimisation of the calcination temperature in order to improve its electrocatalytic activity.

3.2. *Influence of the calcination temperature*

Sample 17.5-BrGOA was carbonized between 400 and 800 °C and obtained materials were characterized in detail. Table 4 presents the elemental composition of the calcined boron-doped graphene aerogels. As can be observed, the thermal reduction of functional oxygen groups only started at calcination temperatures up to 600 °C [49]. Analyses also show that boron doping is clearly reduced compared to the uncalcined sample.

Fig. S4 shows the FTIR analysis corresponding to the synthesized samples. The peak located at 3220 cm^{-1} corresponding to the B–O

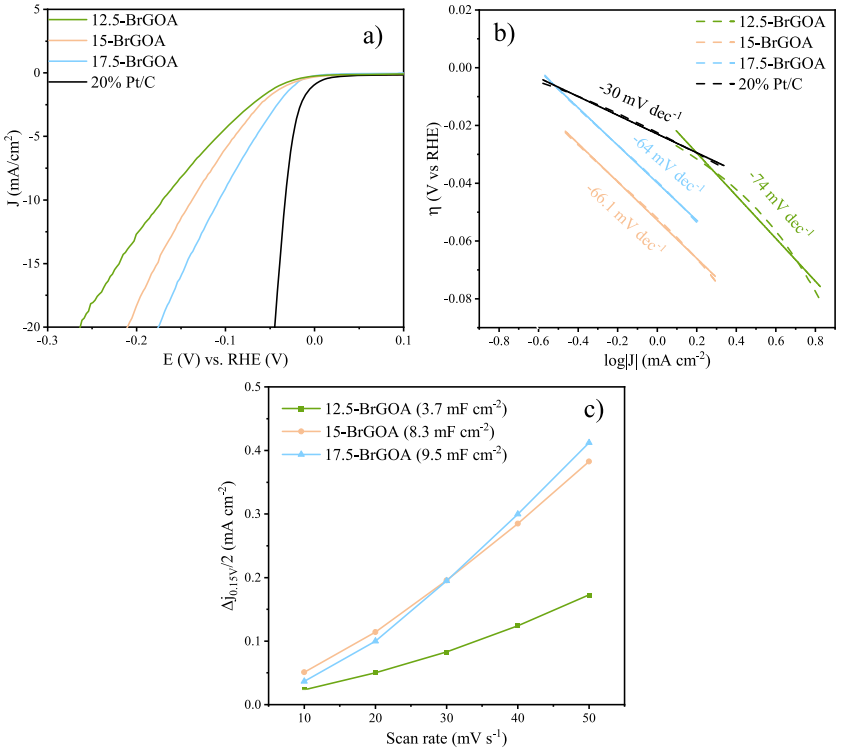

Fig. 5. a) Linear Sweep Voltammetry, b) the corresponding Tafel plots of boron-doped graphene-based aerogels and c) plot of the difference of anodic and cathodic current densities vs. scan rate (0.5 M H_2SO_4 acid media).

Table 4
Elemental composition (wt.%) of 17.5-BrGOA calcined at different temperatures.

Samples	C	H	O	B
Not calcinated	64	2	27	7
400B	68	1	27	4
600B	67	1	27	5
800B	73	1	22	4

[38] confirms the presence of boron and corroborate the information given by elemental composition. The peaks corresponding to the different oxygen functional groups (C═O, C–O–C, C–OH and C–O) showed no significant differences between the samples.

Table 5 shows the physicochemical properties and Fig. S5 the XRD analysis of sample 17.5-BrGOA calcined at different temperatures. It can be observed how the crystallographic parameters L_A and L_C slightly increased with the calcination temperature, indicating a slight increase in the degree of graphitization of the samples. As for the surface area, it increased after calcination due to the removal of carbonaceous residue during carbonization, reaching 198 m^2/g in the sample calcined at 600 °C. This allows us to obtain a high number of pores in the aerogel, which is expected to improve its electrochemical behaviour in HER [50]. This carbonaceous residue is responsible for blocking the pores causing a decrease in both the BET surface area and pore volume [51]. As observed, the surface area and pore volume values of the sample calcined at 800 °C showed a small decrease, probably due to the onset of thermal collapse of the pore structure [52]. Fig. S6 shows the N_2 adsorption-desorption isotherms and Fig. 6 (a - d) shows the pore size distribution of the graphene aerogels calcined at different temperatures. As observed, the increase of the calcination temperature causes a clear increase in mesopores, reaching a maximum at 600 °C and decreasing at high calcination temperatures (800 °C).

Fig. 7 (a - d) and Table 6 show the typology of the boron functional groups incorporated into the carbon network depending on the calcination temperature. Additionally, Fig. S7 shows the XPS survey spectra of 17.5-BrGOA. As observed, the B1 peak reached its minimum when the sample was calcined at 800 °C (3 % of B–O bond) with a surface oxygen presence of 10 %. This confirms that fewer oxygen functional groups are obtained on the surface of the aerogel at higher calcination temperatures, leading to its graphitization [53]. On the other hand, the amount of surface B decreased in the calcined samples, which makes sense considering that the calcination process also eliminates oxygenated functional groups. Furthermore, at high temperatures (800 °C) the carbonaceous structure starts to degrade along with the B bonds. This is shown in the XPS spectra by the decrease in the binding energy of the boron bonds [46], leading the maximum decrease in binding energy at 800 °C for both B–O (from 193.7 to 190.5 eV) and BC_2O (from 192.6 to 188.7 eV) at 800 °C.

Table 5
Crystallographic parameters, textural properties, and density of 17.5-BrGOA calcined at different temperatures.

Samples	L_C (nm)	L_A (nm)	Total pore volume (cm^3/g)	Surface area (m^2/g)	Density (mg/cm^3)
Not calcinated	1.4	3.8	1.1	163	1.1
400B	1.4	3.8	1.2	179	0.9
600B	1.6	4.0	1.3	198	0.8
800B	1.7	4.3	1.4	170	0.9

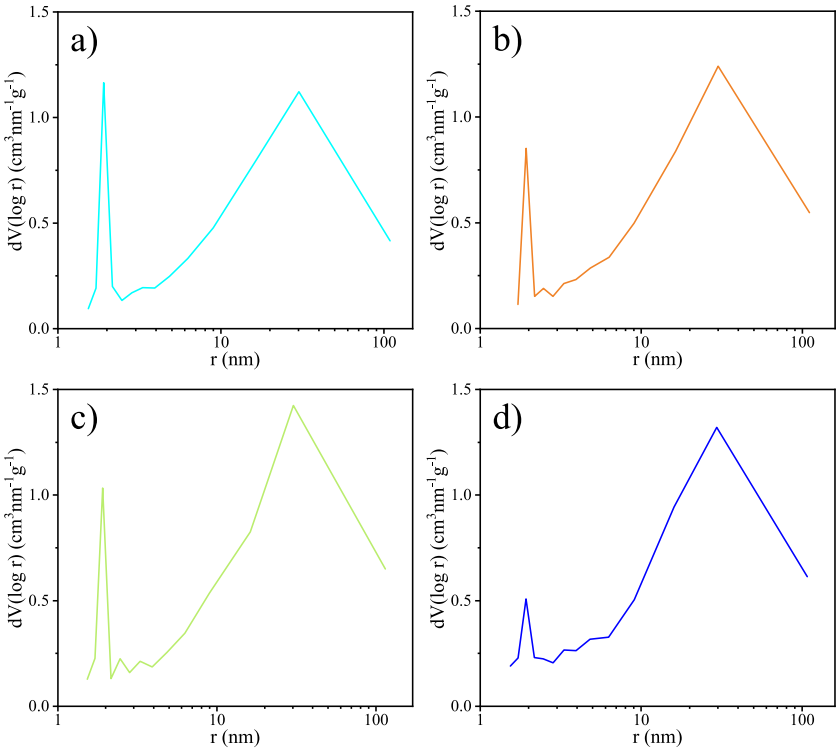

Fig. 6. Pore size distribution of a) 17.5-BrGOA (Not calcined), b) 400B, c) 600B and d) 800B.

Finally, the electrochemical behaviour in HER of the obtained materials is presented in Fig. 8. The metal-free aerogel with the best electrocatalytic results was the sample calcined at 600 °C ($\eta_{10} = 55$ mV) (Fig. 8a), having similar activity to the commercial 20%Pt/C catalyst ($\eta_{10} = 47$ mV) [54]. Calcination modulates the structure of the material by immobilizing reagents in their active form onto the substrate, and by increasing the number of defects and surface area through the decomposition of residues on its surface [55–58]. To study the mechanism of the reaction, Tafel slopes were obtained (Fig. 8b). Tafel slope of samples calcined at 400 °C and 600 °C were quite similar (−59.7 and −58.4 mV dec^{-1}, respectively), and were not very different from that of the commercial 20%Pt/C (−30 mV dec^{-1}) [54] showing the Heyrovsky mechanism reaction in the surface of the electrode. However, a Tafel slope of −124 mV dec^{-1} was achieved at 800 °C showing this electrocatalyst the Volmer's reaction on the surface [59]. This poor performance was predictable due to the bad physicochemical and morphological properties mentioned before. Finally, to confirm the electrochemical behaviour, C_{dl} measurements (obtained of the CVs essays, Fig. S8) were conducted (Fig. 8c). These analyses showed how the sample with higher C_{dl} (600B sample, 13.5 mF cm^{-2}) achieved also better LSV results, obtaining comparable electrochemical behaviour to commercial 20% Pt/C, and C_{dl} values higher than those of other metal-free electrocatalysts reported in literature [60–63]. It is also noted that, as the scan rate is gradually increased, the cyclic voltammograms retain almost the same shape, indicating that the sample calcined at 600 °C has good rate capability [64]. Finally, the repeatability and stability of the optimum 600B sample is shown in Fig. 8d. As observed, the electrochemical activity of the catalyst does not significantly decrease with repetition up to 60 LSVs, making it an electrochemically stable material with high repeatability.

Finally, an in-depth analysis of the most recent bibliography was made up and summarized in Table 7. As can be observed, nearly all the electrocatalysts studied in the literature are calcined at temperatures ranging from 550 to 1050 °C. Among all of them, this work has obtained electrocatalysts (BrGOA) with very low η_{10} values with very good electrochemical activity.

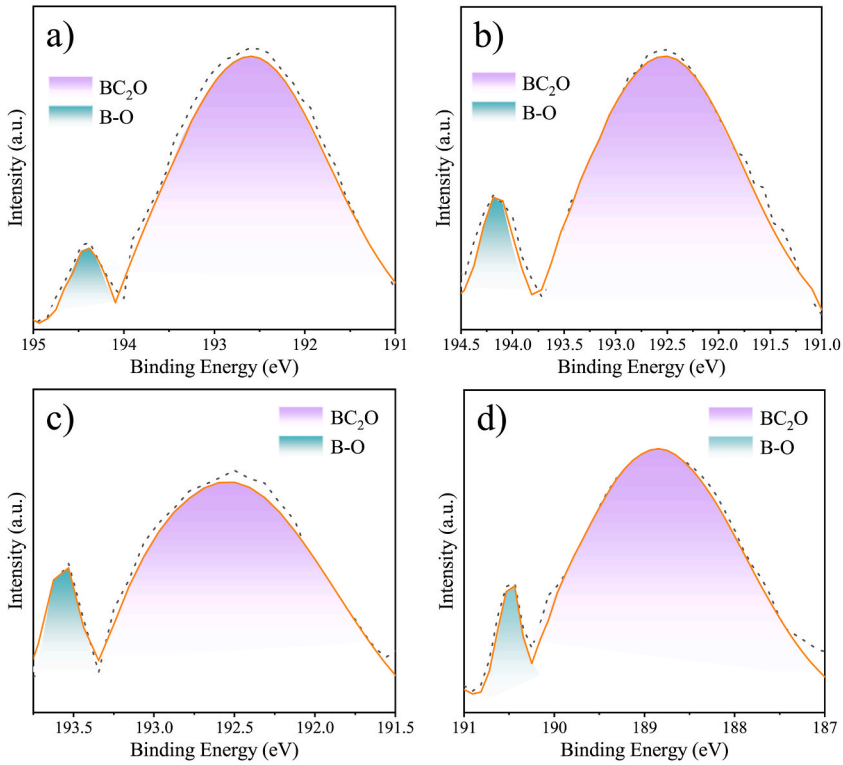

Fig. 7. Core level high-resolution B1s XPS spectra a) 17.5-BrGOA and its calcined derivatives b) 400B, c) 600B and d) 800B.

Table 6
Element content (%) and fitted results of B1s core level XPS spectra of 17.5-BrGOA calcined at different temperatures.

	Element content (%)			% Boron functional groups (BE, eV)[a]	
Samples	C	O	B	B1 (193.7)	B2 (192.6)
Not calcinated	74	21	5	10	90
400B	83	15	2	6	94
600B	84	14	2	5	95
800B	89	10	1	3	97

[a] Notes. B1: B–O, B2: BC_2O.

4. Conclusions

Promising metal-free electrocatalysts based on boron-doped graphene aerogels were successfully synthesized *via* one-step autoclave assembly and freeze-drying. The amount of boric acid used both as a dopant and reducing agent in the synthesis was optimized in order to improve the electrocatalytic activity of the final aerogel (boric acid/GO mass ratio = 17.5) to practically reach the crystallization limit of boric acid (boric acid/GO mass ratio = 20). Furthermore, calcination of the boron-doped electrocatalyst at 600 °C resulted in low oxygen content, moderate surface area, bimodal pore size distribution, and a high number of electrochemical active surface area. The final optimized boron-doped graphene-based aerogel showed electrochemical performance in acid media (η_{10} = 55 mV) resembling that of a 20 % Pt/C commercial catalyst.

Data availability statement

The data that has been used is confidential.

CRediT authorship contribution statement

J. Cencerrero: Conceptualization, Data curation, Formal analysis, Investigation, Methodology, Project administration, Resources, Software, Validation, Visualization, Writing – original draft, Writing – review & editing. **P. Sánchez:** Conceptualization, Investigation, Project administration, Resources, Supervision, Validation, Visualization, Writing – original draft, Writing – review & editing. **A. de**

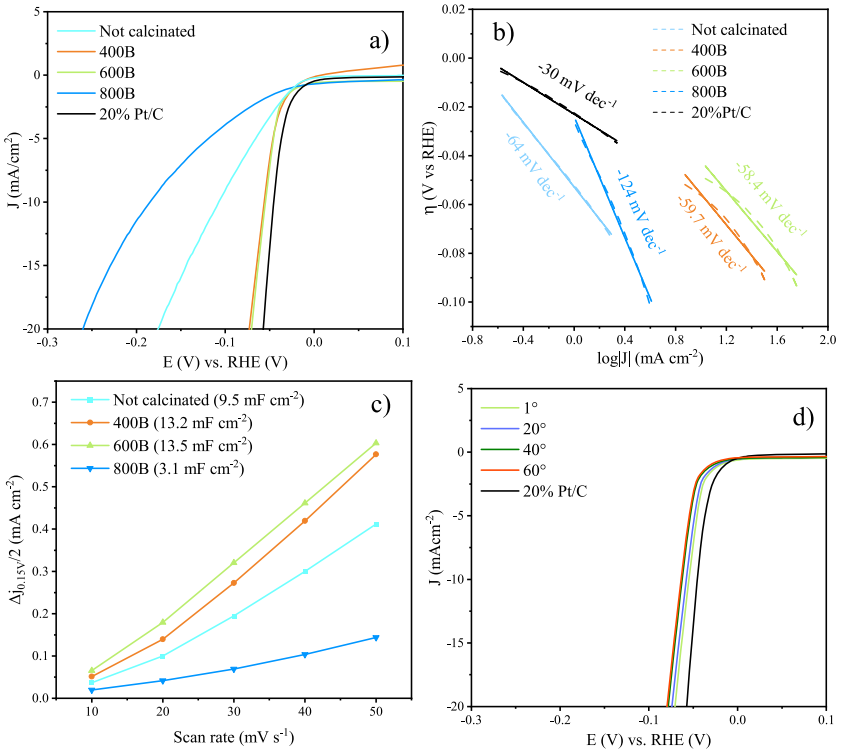

Fig. 8. a) Linear Sweep Voltammetry of 17.5-BrGOA and its calcined samples, b) the corresponding Tafel plots and c) plot of the difference of anodic and cathodic current densities vs. scan rate (0.5 M H_2SO_4 acid media) and d) LSVs tests for the stability of 600B.

Table 7
Comparison of HER activities of metal-free heteroatom-doped graphene-based electrocatalysts (0.5 M H_2SO_4).

Material[a]	Temperature of calcination (°C)	Dopant	η_{10} (Overpotential (mV) at 10 mA cm^{-2})	Reference
C_3N_4@NG	550	N	80	[65]
3DNG-P	800	N,P	128	[66]
DDGM	850	N	245	[67]
S-rGO	–	S	254	[68]
CN/BG	600	B,N	260	[69]
GNW	750	S	310	[70]
BCN@GC	1050	B,N	333	[71]
BrGOA	600	B	55	This work

[a] C_3N_4@NG = C_3N_4 nanolayers with nitrogen-doped graphene sheets; 3DNG-P = 3D N-doped plasma-etched graphene oxide; DDGM = dual defective graphene-based material; S-rGO = Poly-sulfide functionalized reduced graphene; CN/BG = Graphite carbon nitride layer on boron doped graphene; GNW = Graphene nanowall; BCN@GC = graphene capsule-decorated boron-carbon-nitride.

Lucas-Consuegra: Investigation, Project administration, Resources, Supervision. **A.R. de la Osa:** Investigation, Project administration, Resources, Supervision, Writing – review & editing. **A. Romero:** Conceptualization, Investigation, Project administration, Resources, Supervision, Validation, Visualization, Writing – original draft, Writing – review & editing.

Declaration of competing interest

The authors declare that they have no known competing financial interests or personal relationships that could have appeared to influence the work reported in this paper.

Acknowledgements

We gratefully acknowledge the Spanish Ministry of Science and Innovation (Project PID2019-107499RB-100) and FPI grant (BES-2020-093865) for the financial support.

Appendix A. Supplementary data

Supplementary data to this article can be found online at https://doi.org/10.1016/j.heliyon.2023.e20748.

References

[1] Y. Ding, K.W. Cao, J.W. He, F.M. Li, H. Huang, P. Chen, Y. Chen, Nitrogen-doped graphene aerogel-supported ruthenium nanocrystals for pH-universal hydrogen evolution reaction, Chin. J. Catal. 43 (2022) 1535–1543, https://doi.org/10.1016/S1872-2067(21)63977-3.

[2] M.K. Debe, Electrocatalyst approaches and challenges for automotive fuel cells, 486 (2012), Nature 486 (7401) (2012) 43–51, https://doi.org/10.1038/nature11115.

[3] Z. Abdin, A. Zafaranloo, A. Rafiee, W. Mérida, W. Lipiński, K.R. Khalilpour, Hydrogen as an energy vector, Renew. Sustain. Energy Rev. 120 (2020), 109620, https://doi.org/10.1016/J.RSER.2019.109620.

[4] Z. Yin, J. Liang, Z.Y. Zhang, H. Luo, J. Zhou, Construction of superhydrophilic metal-organic frameworks with hierarchical microstructure for efficient overall water splitting, J. Colloid Interface Sci. 623 (2022) 405–416, https://doi.org/10.1016/J.JCIS.2022.05.057.

[5] T. Matthews, T.A. Mashola, K.A. Adegoke, K. Mugadza, C.T. Fakude, O.R. Adegoke, A.S. Adekunle, P. Ndungu, N.W. Maxakato, Electrocatalytic activity on single atoms catalysts: synthesis strategies, characterization, classification, and energy conversion applications, Coord. Chem. Rev. 467 (2022), https://doi.org/10.1016/J.CCR.2022.214600.

[6] A.P. Murthy, J. Theerthagiri, K. Premnath, J. Madhavan, K. Murugan, Single-step electrodeposited molybdenum incorporated nickel sulfide thin films from low-cost precursors as highly efficient hydrogen evolution electrocatalysts in acid medium, J. Phys. Chem. C 121 (2017) 11108–11116, https://doi.org/10.1021/ACS.JPCC.7B02088/ASSET/IMAGES/LARGE/JP-2017-02088J_0007. JPEG.

[7] J. Bai, N. Jia, P. Jin, P. Chen, J.X. Jiang, J.H. Zeng, Y. Chen, Metal-organic interface engineering for boosting the electroactivity of Pt nanodendrites for hydrogen production, J. Energy Chem. 51 (2020) 105–112, https://doi.org/10.1016/J.JECHEM.2020.03.054.

[8] H.Y. Sun, G.R. Xu, F.M. Li, Q.L. Hong, P.J. Jin, P. Chen, Y. Chen, Hydrogen generation from ammonia electrolysis on bifunctional platinum nanocubes electrocatalysts, J. Energy Chem. 47 (2020) 234–240, https://doi.org/10.1016/J.JECHEM.2020.01.035.

[9] W. Li, F. Wang, X. shan Chu, Y. yan Dang, X. yun Liu, T. Ma, J. yuan Li, C. yi Wang, 3D porous BN/rGO skeleton embedded by MoS2 nanostructures for simulated-solar-light induced hydrogen production, Chem. Eng. J. 435 (2022), 132441, https://doi.org/10.1016/J.CEJ.2021.132441.

[10] W. Li, Q. Ma, X. Wang, X.S. Chu, F. Wang, X.C. Wang, C.Y. Wang, Enhanced photoresponse and fast charge transfer: three-dimensional macroporous g-C3N4/GO-TiO2 nanostructure for hydrogen evolution, J Mater Chem A Mater 8 (2020) 19533–19543, https://doi.org/10.1039/D0TA07178A.

[11] W. Li, Y. Dang, T. Ma, J. Li, G. Liao, F. Gao, W. Duan, X. Wang, C. Wang, Synergistic electric metal (Ni SAs)-semiconductor (CdS NPs) interaction for improved H2O-to-H2 conversion performance under simulated sunlight, Sol. RRL 7 (2023), 2300110, https://doi.org/10.1002/SOLR.202300110.

[12] X. li Hao, X. shan Chu, X. yun Liu, W. Li, Synergetic metal-semiconductor interaction: single-atomic Pt decorated CdS nano-photocatalyst for highly water-to-hydrogen conversion, J. Colloid Interface Sci. 621 (2022) 160–168, https://doi.org/10.1016/J.JCIS.2022.04.053.

[13] M.G. Ersozoglu, H. Gursu, S. Gumrukcu, A.S. Sarac, Y. Sahin, Single step electrochemical semi-exfoliated S-doped graphene-like structures from commercial carbon fiber as efficient metal-free catalyst for hydrogen evolution reaction, Chemelectrochem 9 (2022), https://doi.org/10.1002/CELC.202101455.

[14] Y. Wu, J. Zhu, L. Huang, A review of three-dimensional graphene-based materials: synthesis and applications to energy conversion/storage and environment, Carbon N Y 143 (2019) 610–640, https://doi.org/10.1016/J.CARBON.2018.11.053.

[15] J. Cencerrero Fernández del Moral, A. Romero Izquierdo, P. Sánchez Paredes, O. Avilés-García, I. Fernandez-Reina,New Advances in Graphene-Based Three-Dimensional Structures: Synthesis and Applications, Https://Services.Igi-Global.Com/Resolvedoi/Resolve.Aspx?Doi=10.4018/978-1-7998-8936-6.Ch005. (1AD) 101–128. https://doi.org/10.4018/978-1-7998-8936-6.CH005..

[16] Y. Xu, K. Sheng, C. Li, G. Shi, Self-assembled graphene hydrogel via a one-step hydrothermal process, ACS Nano 4 (2010) 4324–4330, https://doi.org/10.1021/NN101187Z/SUPPL_FILE/NN101187Z_SI_001.PDF.

[17] J. Xie, L. Niu, Y. Qiao, P. Chen, D. Rittel, Impact energy absorption behavior of graphene aerogels prepared by different drying methods, Mater. Des. 221 (2022), https://doi.org/10.1016/J.MATDES.2022.110912.

[18] Y.F. Wang, S.J. Zou, W.P. Hu, F.F. Wu, J.X. Yang, Y.Y. Cen, D.X. Yang, Z.Q. Hou, K.J. Huang, Biomass-derived graphene-like carbon nanoflakes for advanced supercapacitor and hydrogen evolution reaction, J. Alloys Compd. 928 (2022), https://doi.org/10.1016/J.JALLCOM.2022.167176.

[19] W. Wu, M. Du, H. Shi, Q. Zheng, Z. Bai, Application of Graphene Aerogels in Oil Spill Recovery: A Review, Science of The Total Environment, 2022, 159107, https://doi.org/10.1016/J.SCITOTENV.2022.159107.

[20] J. Cencerrero, P. Sánchez, A. de Lucas-Consuegra, A.R. de la Osa, A. Romero, Influence of the reducing agent on the physicochemical and electrocatalytic properties of graphene-based aerogels, FlatChem 36 (2022), 100435, https://doi.org/10.1016/J.FLATC.2022.100435.

[21] X.R. Wang, J.Y. Liu, Z.W. Liu, W.C. Wang, J. Luo, X.P. Han, X.W. Du, S.Z. Qiao, J. Yang, Identifying the key role of pyridinic-N–Co bonding in synergistic electrocatalysis for reversible ORR/OER, Adv. Mater. 30 (2018), 1800005, https://doi.org/10.1002/ADMA.201800005.

[22] W.T. Chen, D. Dutta, Y.H. Hung, Y.Y. Sin, S.M. He, J.K. Chang, C.Y. Su, Designed catalytic protocol for enhancing hydrogen evolution reaction performance of P, N-Co-doped graphene: the correlation of manipulating the dopant allocations and heteroatomic structure, J. Phys. Chem. C 124 (2020) 25701–25711, https://doi.org/10.1021/ACS.JPCC.0C07467/ASSET/IMAGES/MEDIUM/JP0C07467_M001. GIF.

[23] J. Zhou, F. Qi, Y. Chen, Z. Wang, B. Zheng, X. Wang, CVD-grown three-dimensional sulfur-doped graphene as a binder-free electrocatalytic electrode for highly effective and stable hydrogen evolution reaction, J. Mater. Sci. 53 (2018) 7767–7777, https://doi.org/10.1007/S10853-018-2118-6.

[24] L. Yang, X. Wang, J. Wang, G. Cui, D. Liu, Graphite carbon nitride/boron-doped graphene hybrid for efficient hydrogen generation reaction, Nanotechnology 29 (2018), https://doi.org/10.1088/1361-6528/AAC9AE.

[25] Y. Li, C. Ai, S. Deng, Y. Wang, X. Tong, X. Wang, X. Xia, J. Tu, Nitrogen doped vertical graphene as metal-free electrocatalyst for hydrogen evolution reaction, Mater. Res. Bull. 134 (2021), https://doi.org/10.1016/J.MATERRESBULL.2020.111094.

[26] R. Kumar, S. Sahoo, E. Joanni, R.K. Singh, K. Maegawa, W.K. Tan, G. Kawamura, K.K. Kar, A. Matsuda, Heteroatom doped graphene engineering for energy storage and conversion, Mater. Today 39 (2020) 47–65, https://doi.org/10.1016/J.MATTOD.2020.04.010.

[27] X.K. Kong, C. le Chen, Q.W. Chen, Doped graphene for metal-free catalysis, Chem. Soc. Rev. 43 (2014) 2841–2857, https://doi.org/10.1039/C3CS60401B.

[28] J. Zhang, L. Dai, Heteroatom-doped graphitic carbon catalysts for efficient electrocatalysis of oxygen reduction reaction, ACS Catal. 5 (2015) 7244–7253, https://doi.org/10.1021/ACSCATAL.5B01563/ASSET/IMAGES/LARGE/CS-2015-01563F_0007. JPEG.

[29] L. Yang, X. Wang, J. Wang, G. Cui, D. Liu, Graphite carbon nitride/boron-doped graphene hybrid for efficient hydrogen generation reaction, Nanotechnology 29 (2018), 345705, https://doi.org/10.1088/1361-6528/AAC9AE.

[30] R. Nankya, J. Lee, D.O. Opar, H. Jung, Electrochemical behavior of boron-doped mesoporous graphene depending on its boron configuration, Appl. Surf. Sci. 489 (2019) 552–559, https://doi.org/10.1016/J.APSUSC.2019.06.015.

[31] M.P. Lavin-Lopez, A. Paton-Carrero, L. Sanchez-Silva, J.L. Valverde, A. Romero, Influence of the reduction strategy in the synthesis of reduced graphene oxide, Adv. Powder Technol. 28 (2017) 3195–3203, https://doi.org/10.1016/J.APT.2017.09.032.

[32] V. Thirumal, A. Pandurangan, R. Jayavel, R. Ilangovan, Synthesis and characterization of boron doped graphene nanosheets for supercapacitor applications, Synth. Met. 220 (2016) 524–532, https://doi.org/10.1016/J.SYNTHMET.2016.07.011.

[33] L. Wang, X. Duan, X. Liu, J. Gu, R. Si, Y. Qiu, Y. Qiu, D. Shi, F. Chen, X. Sun, J. Lin, J. Sun, X. Liu, J. Gu, R. Si, L. Wang, Y. Qiu, D. Shi, J. Lin, J. Sun, X. Duan, F. Chen, X. Sun, Atomically dispersed Mo supported on metallic Co9S8 nanoflakes as an advanced noble-metal-free bifunctional water splitting catalyst working in universal pH conditions, Adv. Energy Mater. 10 (2020), 1903137, https://doi.org/10.1002/AENM.201903137.

[34] M.A. Ahsan, A.R. Puente Santiago, Y. Hong, N. Zhang, M. Cano, E. Rodriguez-Castellon, L. Echegoyen, S.T. Sreenivasan, J.C. Noveron, Tuning of trifunctional NiCu bimetallic nanoparticles confined in a porous carbon network with surface composition and local structural distortions for the electrocatalytic oxygen reduction, oxygen and hydrogen evolution reactions, J. Am. Chem. Soc. 142 (2020) 14688–14701, https://doi.org/10.1021/JACS.0C06960/SUPPL_FILE/JA0C06960_SI_001.PDF.

[35] A. Paton-Carrero, A.R. de la Osa, P. Sanchez, A. Rodriguez-Gomez, A. Romero, Towards new routes to increase the electrocatalytic activity for oxygen reduction reaction of n-doped graphene nanofibers, J. Electroanal. Chem. 878 (2020), 114631, https://doi.org/10.1016/J.JELECHEM.2020.114631.

[36] B. Lesiak, G. Trykowski, J. Tóth, S. Biniak, L. Kövér, N. Rangam, L. Stobinski, A. Malolepszy, Chemical and structural properties of reduced graphene oxide—dependence on the reducing agent, J. Mater. Sci. 56 (2021) 3738–3754, https://doi.org/10.1007/S10853-020-05461-1/FIGURES/9.

[37] V. Sharma, Y. Jain, M. Kumari, R. Gupta, S.K. Sharma, K. Sachdev, Synthesis and characterization of graphene oxide (GO) and reduced graphene oxide (rGO) for gas sensing application, Macromol. Symp. 376 (2017), 1700006, https://doi.org/10.1002/MASY.201700006.

[38] S. Chowdhury, Y. Jiang, S. Muthukaruppan, R. Balasubramanian, Effect of boron doping level on the photocatalytic activity of graphene aerogels, Carbon N Y 128 (2018) 237–248, https://doi.org/10.1016/J.CARBON.2017.11.089.

[39] R. Yuan, Y. Xu, Y. Wang, F. You, W. Chen, C. Ding, D. Jiang, K. Wang, One-pot hydrothermal preparation of B and N co-doped graphene aerogels loaded with cobalt oxides for the synergistic enhancement of oxygen reduction electrocatalysis, J. Electroanal. Chem. 877 (2020), 114555, https://doi.org/10.1016/J.JELECHEM.2020.114555.

[40] H. Guo, Q. Gao, Boron and nitrogen co-doped porous carbon and its enhanced properties as supercapacitor, J. Power Sources 186 (2009) 551–556, https://doi.org/10.1016/J.JPOWSOUR.2008.10.024.

[41] Y. Guan, Y. Gong, W. Li, J. Gelb, L. Zhang, G. Liu, X. Zhang, X. Song, C. Xia, Y. Xiong, H. Wang, Z. Wu, Y. Tian, Quantitative analysis of micro structural and conductivity evolution of Ni-YSZ anodes during thermal cycling based on nano-computed tomography, J. Power Sources 196 (2011) 10601–10605, https://doi.org/10.1016/J.JPOWSOUR.2011.08.083.

[42] Z. Rahmani, A.M. Rashidi, A. kazemi, M.T. Samadi, A.R. Rahmani, N-doped reduced graphene oxide aerogel for the selective adsorption of oil pollutants from water: isotherm and kinetic study, J. Ind. Eng. Chem. 61 (2018) 416–426, https://doi.org/10.1016/J.JIEC.2017.12.041.

[43] X.-R. Wang, J.-Y. Liu, Z.-W. Liu, W.-C. Wang, J. Luo, X.-P. Han, X.-W. Du, S.-Z. Qiao, J. Yang, G. Hybrids X-R Wang, Z. Liu, X. Du, S. Qiao, J. Yang, J. Liu, W. Wang, J. Luo, X. Han, Identifying the key role of pyridinic-N–Co bonding in synergistic electrocatalysis for reversible ORR/OER, Adv. Mater. 30 (2018), 1800005, https://doi.org/10.1002/ADMA.201800005.

[44] A. Toghan, M. Khairy, M.M. Mohamed, A.A. Amer, Synthesis of defect-impressive boron graphene as a remarkable electrocatalyst for methanol oxidation reaction, J. Mater. Res. Technol. 16 (2022) 362–372, https://doi.org/10.1016/J.JMRT.2021.12.001.

[45] E. Aslan, Z. Eroğlu, G. Yanalak, Ö. Metin, I. Hatay Patir, Enhanced hydrogen evolution via in situ generated 2D black phosphorous nanocomposites at the liquid/liquid interfaces, Appl. Surf. Sci. 604 (2022), https://doi.org/10.1016/J.APSUSC.2022.154435.

[46] P. Joshi, R. Yadav, M. Hara, T. Inoue, Y. Motoyama, M. Yoshimura, Contribution of B,N-co-doped reduced graphene oxide as a catalyst support to the activity of iridium oxide for oxygen evolution reaction, J Mater Chem A Mater 9 (2021) 9066–9080, https://doi.org/10.1039/D1TA00158B.

[47] G. Fu, X. Yan, Y. Chen, L. Xu, D. Sun, J.-M. Lee, Y. Tang, G. Fu, X. Yan, Y. Chen, L. Xu, D. Sun, Y. Tang, J. Lee, Boosting bifunctional oxygen electrocatalysis with 3D graphene aerogel-supported Ni/MnO particles, Adv. Mater. 30 (2018), 1704609, https://doi.org/10.1002/ADMA.201704609.

[48] Y. Tian, Y. Ye, X. Wang, S. Peng, Z. Wei, X. Zhang, W. Liu, Three-dimensional N-doped, plasma-etched graphene: highly active metal-free catalyst for hydrogen evolution reaction, Appl. Catal. Gen. 529 (2017) 127–133, https://doi.org/10.1016/J.APCATA.2016.10.021.

[49] D.G. Trikkaliotis, A.K. Christoforidis, A.C. Mitropoulos, G.Z. Kyzas, Graphene oxide synthesis, properties and characterization techniques: a comprehensive review, ChemEngineering 5 (2021), https://doi.org/10.3390/CHEMENGINEERING5030064.

[50] Y. Guan, Y. Gong, W. Li, J. Gelb, L. Zhang, G. Liu, X. Zhang, X. Song, C. Xia, Y. Xiong, H. Wang, Z. Wu, Y. Tian, Quantitative analysis of micro structural and conductivity evolution of Ni-YSZ anodes during thermal cycling based on nano-computed tomography, J. Power Sources 196 (2011) 10601–10605, https://doi.org/10.1016/J.JPOWSOUR.2011.08.083.

[51] M. Wu, Z. Dou, J. Chang, L. Cui, Nitrogen and sulfur co-doped graphene aerogels as an efficient metal-free catalyst for oxygen reduction reaction in an alkaline solution, RSC Adv. 6 (2016) 22781–22790, https://doi.org/10.1039/C5RA22136F.

[52] C. Wang, Y. Huang, H. Pan, J. Jiang, X. Yang, Z. Xu, H. Tian, S. Han, D. Wu, Nitrogen-doped porous carbon/graphene aerogel with much enhanced capacitive behaviors, Electrochim. Acta 215 (2016) 100–107, https://doi.org/10.1016/J.ELECTACTA.2016.08.077.

[53] X. Zhang, X. Li, Z. Pan, Y. Lai, Y. Lu, Y. Wang, S. Song, Boosting hydrogen evolution electrocatalysis through defect engineering: a strategy of heat and cool shock, Chem. Eng. J. 426 (2021), 131524, https://doi.org/10.1016/J.CEJ.2021.131524.

[54] L. Huang, W. Li, X. Shen, C. Sun, J. Yang, X.R. Shi, M. Zeng, Phosphorus-bridged ternary metal alloy encapsulated in few-layered nitrogen-doped graphene for highly efficient electrocatalytic hydrogen evolution, J Mater Chem A Mater 10 (2022) 7111–7121, https://doi.org/10.1039/D1TA10032G.

[55] G. Lemes, D. Sebastián, E. Pastor, M.J. Lázaro, N-doped graphene catalysts with high nitrogen concentration for the oxygen reduction reaction, J. Power Sources 438 (2019), 227036, https://doi.org/10.1016/J.JPOWSOUR.2019.227036.

[56] X. Zhang, X. Li, Z. Pan, Y. Lai, Y. Lu, Y. Wang, S. Song, Boosting hydrogen evolution electrocatalysis through defect engineering: a strategy of heat and cool shock, Chem. Eng. J. 426 (2021), https://doi.org/10.1016/J.CEJ.2021.131524.

[57] Y. Liu, W. Li, H. Wu, S. Lu, Carbon dots enhance ruthenium nanoparticles for efficient hydrogen production in alkaline, Wuli Huaxue Xuebao/Acta Phys. - Chim. Sin. 37 (2021), https://doi.org/10.3866/PKU.WHXB202009082.

[58] A. Mondal, A. Paul, D.N. Srivastava, A.B. Panda, Defect- and phase-induced acceleration of electrocatalytic hydrogen production by ultrathin and small MoS2-decorated rGO sheets, ACS Appl. Nano Mater. 1 (2018) 4622–4632, https://doi.org/10.1021/ACSANM.8B00914.

[59] F. Bao, E. Kemppainen, I. Dorbandt, R. Bors, F. Xi, R. Schlatmann, R. van de Krol, S. Calnan, Understanding the hydrogen evolution reaction kinetics of electrodeposited nickel-molybdenum in acidic, near-neutral, and alkaline conditions, Chemelectrochem 8 (2021) 195–208, https://doi.org/10.1002/CELC.202001436.

[60] Y. Yang, B. Hu, W. Zhao, Q. Yang, F. Yang, J. Ren, X. Li, Y. Jin, L. Fang, Q. Pan, Bridging N-doped graphene and carbon rich C3N4 layers for photo-promoted multi-functional electrocatalysts, Electrochim. Acta 317 (2019) 25–33, https://doi.org/10.1016/J.ELECTACTA.2019.05.140.

[61] W. Wang, H. Tang, H. Liu, S. Li, Y. Wang, Q. Liu, Ruthenium-based graphene-like layered carbon compos-ites as high-efficiency electrocatalyst for hydrogen evolu-tion reaction, Chem. Phys. Lett. 789 (2022), https://doi.org/10.1016/J.CPLETT.2021.139324.

[62] X. Dao, M. Nie, H. Sun, W. Dong, Z. Xue, Q. Li, J. Liao, X. Wang, X. Zhao, D. Yang, L. Teng, Electrochemical performance of metal-organic framework MOF(Ni) doped graphene, Int. J. Hydrogen Energy 47 (2022) 16741–16749, https://doi.org/10.1016/J.IJHYDENE.2022.03.176.

[63] S.J. Huang, S. Balu, N.R. Barveen, R. Sankar, Surface engineering of reduced graphene oxide onto the nanoforest-like nickel selenide as a high performance electrocatalyst for OER and HER, Colloids Surf. A Physicochem. Eng. Asp. 654 (2022), https://doi.org/10.1016/J.COLSURFA.2022.130024.

[64] W. Tan, R. Fu, H. Ji, Y. Kong, Y. Xu, Y. Qin, Preparation of nitrogen-doped carbon using graphene Quantum dots-chitosan as the precursor and its supercapacitive behaviors, Int. J. Biol. Macromol. 112 (2018) 561–566, https://doi.org/10.1016/J.IJBIOMAC.2018.02.014.

[65] J. Duan, S. Chen, M. Jaroniec, S.Z. Qiao, Porous C3N4 nanolayers@n-graphene films as catalyst electrodes for highly efficient hydrogen evolution, ACS Nano 9 (2015) 931–940, https://doi.org/10.1021/NN506701X/SUPPL_FILE/NN506701X_SI_001.PDF.

[66] Y. Tian, Y. Ye, X. Wang, S. Peng, Z. Wei, X. Zhang, W. Liu, Three-dimensional N-doped, plasma-etched graphene: highly active metal-free catalyst for hydrogen evolution reaction, Appl. Catal. Gen. 529 (2017) 127–133, https://doi.org/10.1016/J.APCATA.2016.10.021.

[67] Y. long Wang, G. qi Sun, L. hua Chen, Z. kai Du, X. yun Li, C. fang Ye, J. ping Liu, B. lian Su, Engineering dual defective graphenes to synergistically improve electrocatalytic hydrogen evolution, Appl. Surf. Sci. 566 (2021), https://doi.org/10.1016/J.APSUSC.2021.150712.

[68] A. Kapuria, T.K. Mondal, B.K. Shaw, Y.K. Su, S.K. Saha, Polysulfide functionalized reduced graphene oxide for electrocatalytic hydrogen evolution reaction and supercapacitor applications, Int. J. Hydrogen Energy (2023), https://doi.org/10.1016/J.IJHYDENE.2023.01.214.
[69] L. Yang, X. Wang, J. Wang, G. Cui, D. Liu, Graphite carbon nitride/boron-doped graphene hybrid for efficient hydrogen generation reaction, Nanotechnology 29 (2018), 345705, https://doi.org/10.1088/1361-6528/AAC9AE.
[70] S. Chaitoglou, R. Amade, E. Bertran, Insights into the inherent properties of vertical graphene flakes towards hydrogen evolution reaction, Appl. Surf. Sci. 592 (2022), https://doi.org/10.1016/J.APSUSC.2022.153327.
[71] Y. Liu, R. Ali, J. Ma, W. Jiao, L. Yin, C. Mu, X. Jian, Graphene-decorated boron-carbon-nitride-based metal-free catalysts for an enhanced hydrogen evolution reaction, ACS Appl. Energy Mater. 4 (2021) 3861–3868, https://doi.org/10.1021/ACSAEM.1C00238.